Results from a Pre-Clinical Head Scanner for Proton CT

Hartmut F.-W. Sadrozinski, for the pCT Collaboration:

R. P. Johnson, Tia Plautz, Hartmut F.-W. Sadrozinski, A. Zatserklyaniy: *SCIPP, U.C. Santa Cruz, Santa Cruz, CA , USA*

V. Bashkirov, V. Giacometti, F. Hurley, P. Piersimoni, R. Schulte: *Division of Radiation Research, Loma Linda University, Loma Linda, CA, USA*

P. Karbasi, K. Schubert, B.Schultze: *Baylor University, Waco, TX, USA*

LOMA LINDA UNIVERSITY HEALTH

BAYLOR UNIVERSITY

Example 200 MeV Proton Event

The noise level seen in the tracker in this event (i.e. zero noise hits) is typical. Only a few strips out of 9216 have an electronics noise occupancy measuring above 1 hit per million triggers.

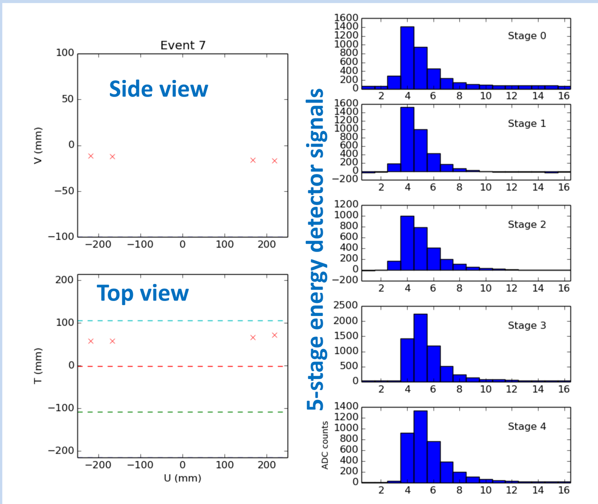

Above is a display of the raw data from a single proton event, with no phantom present on the rotation stage. On the left are plotted the positions of all SSD strips above threshold in both VU and TU views. On the right are plotted 16 14-bit ADC samples for each of the five scintillators. The 200 MeV proton stopped in Stage 4. Note that this event is from a diagnostic run in which the individual ADC samples were written out. Each bin represents ~15 ns. Normally the pulses are reduced in the front-end FPGA to just a pulse-size sum for each of the five scintillators.

Summary

Proton CT (pCT) is an evolving technology that promises to improve proton treatment planning by addressing the range uncertainty problem. Proton CT will generate a set of integrated relative stopping power (RSP) measurements that are used to reconstruct a map of RSP values to be input into a treatment planning system. Our NIH funded pCT Collaboration has built and successfully operated a Phase-II scanner that was designed to measure *individually* at least one million protons per second, more than 50 times faster than our previous Phase-I device. At this rate a full scan can be completed in less than 10 minutes, a performance level that will allow us to complete a full pre-clinical performance evaluation of this new modality. Here we report on the hardware implementation, initial testing and first image reconstruction.

Our Phase-II scanner is based on two silicon-strip tracking-detector modules, an energy/range detector based on 5 scintillator stages read out by photomultiplier tubes, a rotating stage, and a custom high-speed data acquisition system based on 16 FPGAs.

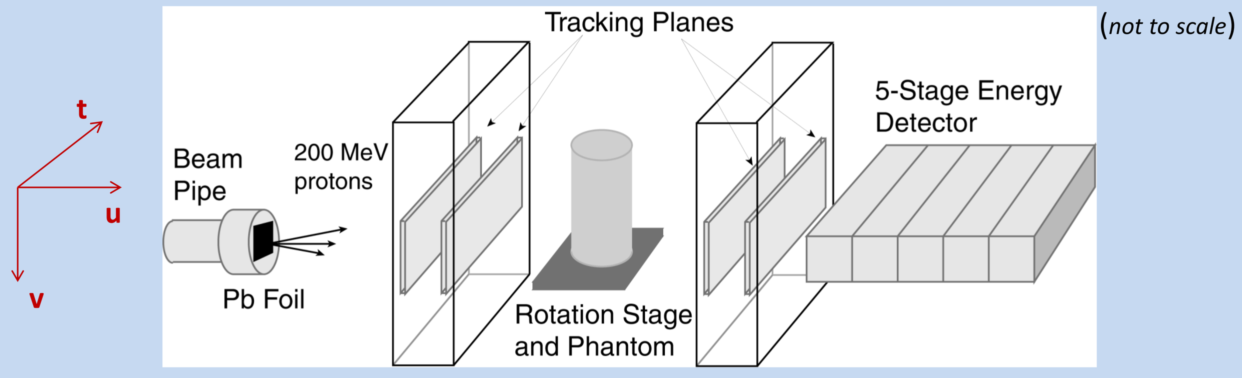

H.F.-W. Sadrozinski, et al, *Development of a Head Scanner for Proton CT*, Nucl. Instr. Meth. A 699 (2013) 205.

pCT Scanner in the CDH Proton Beam Line

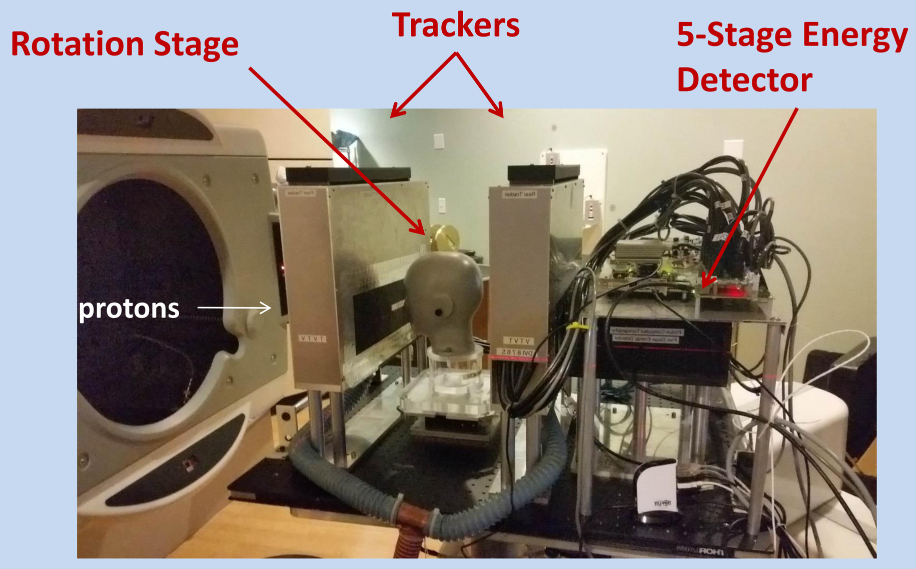

The pCT scanner consists of two trackers, one preceding and one following the object being imaged, and an energy/range detector that measures the Water Equivalent Path Length (WEPL) of the material through which the proton passed in traversing the object. Together, the two trackers measure the incoming and outgoing proton trajectories, from which the geometric path through the object can be estimated. The stage rotates the object being imaged.

Tracking Technology

Silicon strip detectors are nearly ideal candidates for the tracking portion of a pCT system. The relatively high cost per cm² of the sensors (compared to plastic scintillators, for example) is more than offset by their high performance, reliability, stability, and ease of assembly. Furthermore, the sensor cost would be a minor portion of the overall cost of a clinical system. Silicon strip detectors offer the following attractive characteristics, demonstrated in very large systems such as the Fermi-LAT Gamma-ray Space Telescope and the CERN LHC tracking detectors:

- *Near 100% efficiency for charged particle detection with practically zero noise occupancy.*
- *Inherently fine spatial resolution (about 70 microns rms in this case).*
- *Simple calibration that is stable over time periods of many years.*
- *Compact and easy assembly using standard mechanized industrial processes, with excellent mechanical stability.*

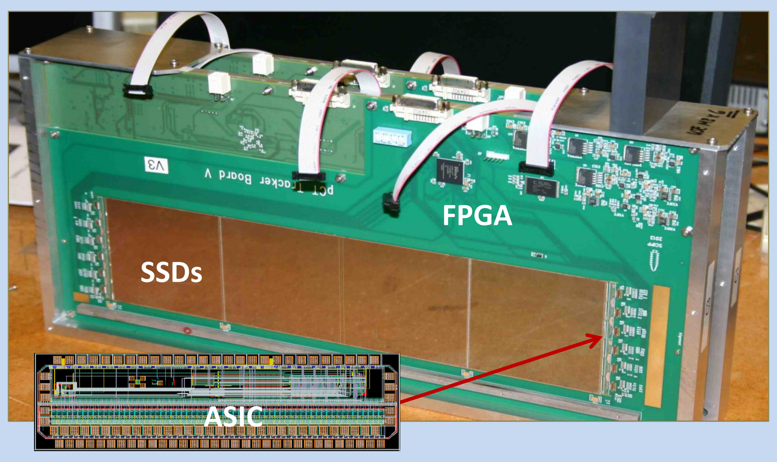

Photograph of one tracking detector assembly with 4 layers of silicon-strip detectors. A "V" layer, which measures the vertical coordinate, is visible in front. Signals from 64 strips are amplified, digitized, and read out by each custom IC (inset). A Xilinx Spartan-6 FPGA controls the setup and readout, assembles the data from the 12 front-end ICs, and transmits the data to the event builder over a DVI-D cable at a rate of 100 Mbit/s. The loose cables visible here are used to program the 6 FPGAs (1 on each "V" board and 2 on each "T" board). An I²C bus on each board monitors temperature as well as the voltages and currents for each voltage regulator, plus the current for the 100 V SSD bias. The use of "slim-edge" technology reduces the dead region around SSD joints to less than 0.6 mm in width.

Hit efficiency with gaps regions included = 99.4%

R. Johnson et al, *Tracker Readout ASIC for Proton Computed Tomography Data Acquisition*, IEEE Trans. Nucl. Sci. **60**, 3262-3269, 2013.

pCT Data Acquisition (DAQ) Flow

The readout is triggered, for ease of synchronization and event building, with ample buffering at the front end to minimize dead time. Eight layers of silicon strip detectors are read out by 144 64-channel ICs, each with a 100 Mbit/s link to an FPGA on the same board. Similarly, each of the two energy detector boards includes an FPGA. The 14 front-end Spartan-6 FPGAs build the local event data and then send it over dual-link DVI-D cables to the Virtex-6 FPGA, which builds the complete event and then sends it by Ethernet to a computer that is running a custom Python-coded DAQ program.

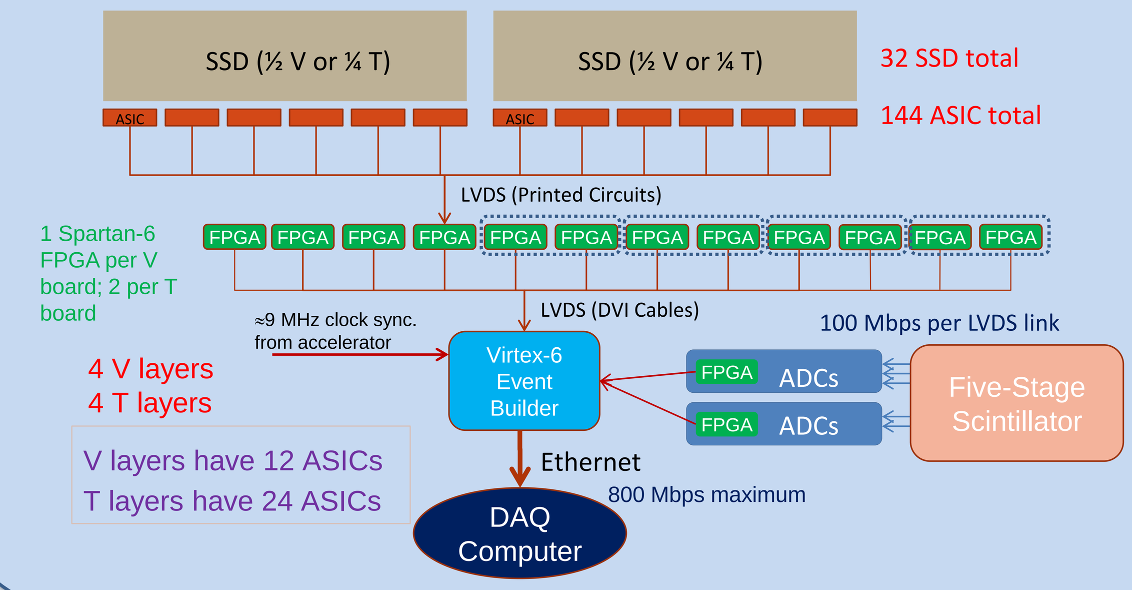

5-Stage Energy/Range Detector

Dividing the energy detector into 5 stages greatly reduces the requirement on energy resolution, allowing effective use of fast plastic scintillators. Stages through which the proton passes directly measure contributions to total range, so the last segment, in which the proton stops, need measure only a small residual range, with only a relaxed precision requirement.

Each custom board shown below digitizes the signals from three scintillator-PMT pairs (see the photograph at left). Each 14-bit ADC can operate at rates up to 65 MHz. The FPGA buffers the data and, upon receipt of a trigger, reduces the data by summing 6 samples around the peak of the pulse (1 before and 4 after). A separate amplifier-discriminator chain in each channel provides asynchronous signals for the trigger logic.

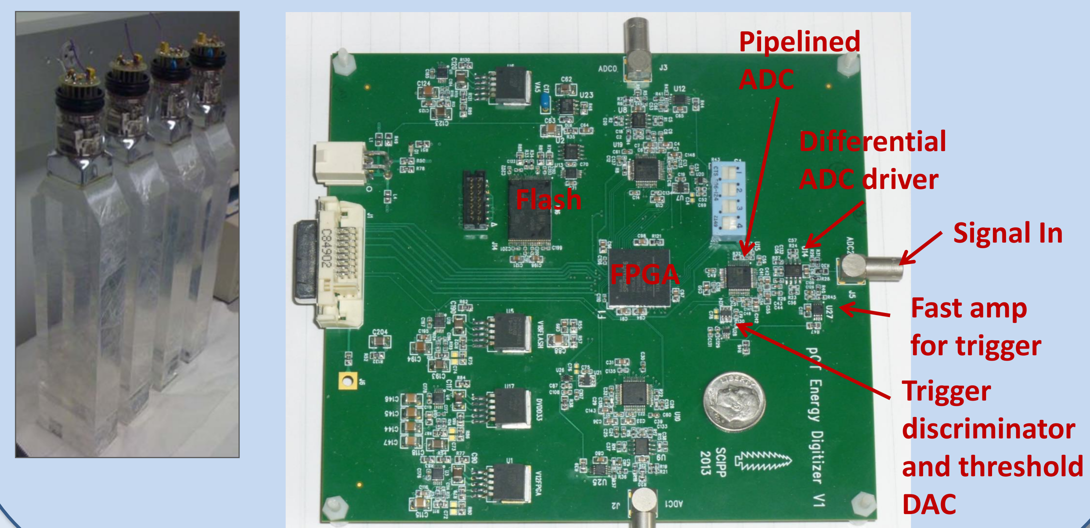

Spatial Resolution Studies: Edge Phantom

A phantom was designed and fabricated for the purpose of measuring a **modulation transfer function (MTF)**

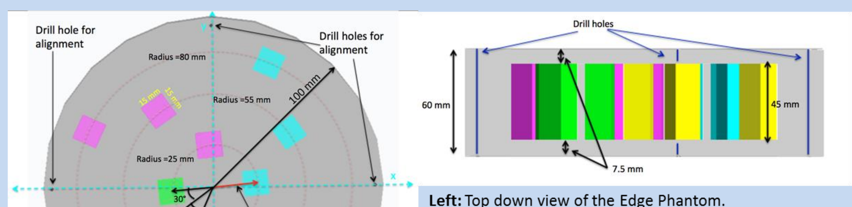

Left: Top down view of the Edge Phantom.
Right: Side view of the Edge Phantom

Cyan: Tooth Enamel
$\rho = 2.04$ g/cm³; RSP = 1.784
Magenta: Cortical Bone
$\rho \sim 1.91$ g/cm³; RSP = 1.699
Green: Lung
$\rho \sim 0.205$ g/cm³; RSP = 0.203
Yellow: Air
$\rho = 0.0012$ g/cm³; RSP = 1.06e-03

MTF is the function of relative modulation with respect to spatial frequency (lp/cm) that characterizes the resolution of an imaging system.

July 2015, CDH: 7 min continuous scan (1 rev/min), 150 Million histories, 1 mm x 1 mm x 1 mm voxel size, 1 deg angular bin size.

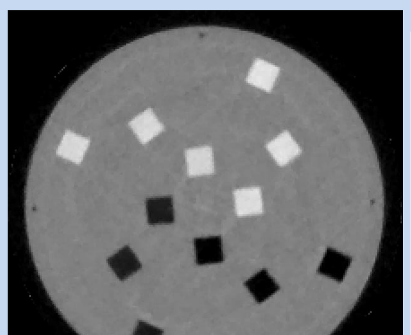

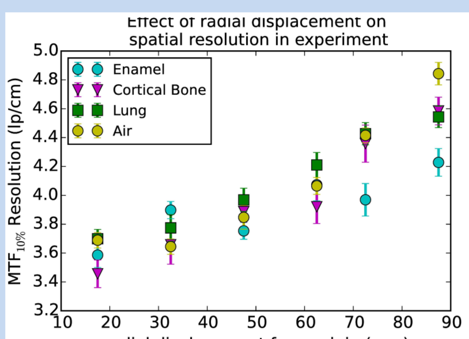

Spatial Resolution is close to maximum (for 1mm pixels the Nyquist frequency is 5 lp/cm).

MTF varies as a function of radius by ± 10-20%.

T. Plautz, IUPESM World Congress 2015, Toronto, ON

DAQ Performance

The system performs as designed, with a sustained rate of more than a million proton events acquired per second and trigger rates much higher than the maximum data acquisition rate., as illustrated here for both LLU and CDH beams.

In the most recent beam test, 2.5 billion events with a total of $1.8{\times}10^{11}$ bytes were acquired with zero CRC errors in the data stream, zero parity errors in the command streams, and zero event building errors.

Operations at Loma Linda U. (LLU) Synchrotron

Spill 2.3 sec on. 2.3 sec off, Beam microstructure of ~100ns.

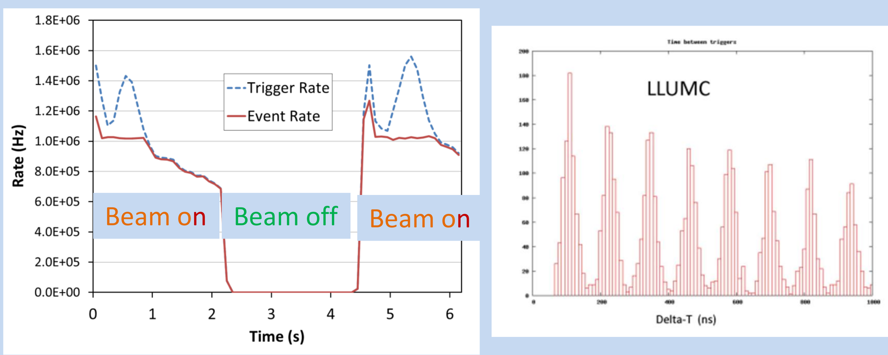

Rotational scan in steps of 2° or 4° during beam-off time

Operations at Central DuPage Hospital (CDH) Cyclotron

Continuous beam with small intensity modulations

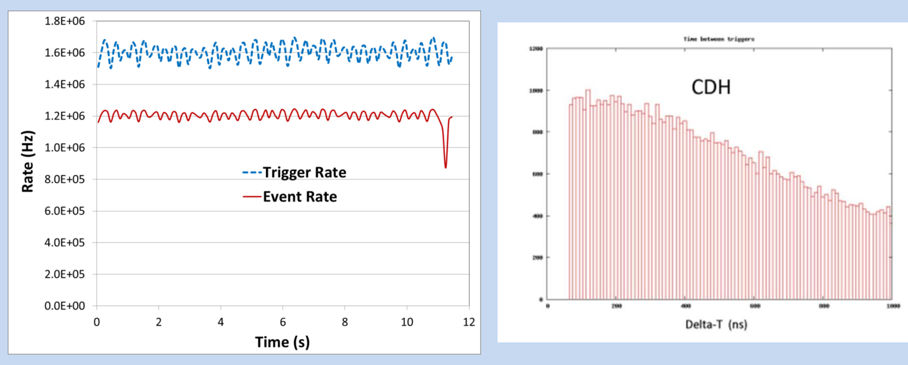

Continuous rotational scan with 1 rev./min.
1. Real-time alignment
2. Optimization of binning for reconstruction.

Goal of sustained MHz+ operation has been reached (even at higher trigger rates)!

WEPL Calibration

A polystyrene "phantom" with 3 stepped pyramids is used to calibrate the measurement of Water Equivalent Path Length (WEPL). In practice separate runs are executed with the stepped pyramids combined with 0, 1, 2, 3, or 4 polystyrene blocks. The tracking system is used to correlate each proton track with the correct step and with the reconstructed signals from the energy/range detector. The result is that the WEPL of each proton can be reconstructed to an rms precision of 3 mm, close to the theoretical limit due to stochastic range straggling of 2.75 mm for 200 MeV protons.

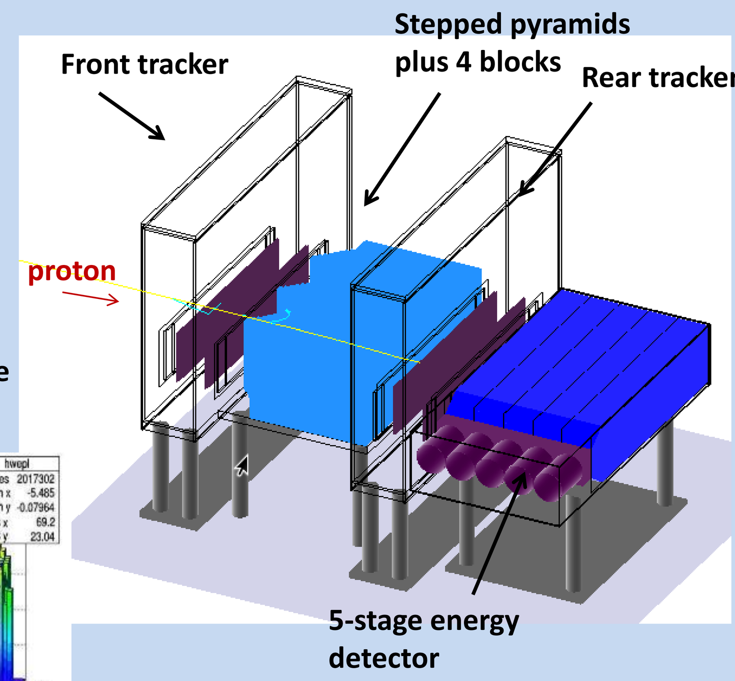

Reconstructed WEPL of the phantom after calibration.

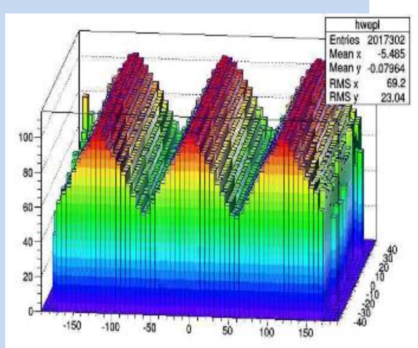

V. Bashkirov et al., *Novel scintillation detector design and performance for proton radiography and computed tomography*, Medical Physics (in print)

Proton CT Image Reconstruction

The CATPHAN 404 phantom is reconstructed from 200 MeV proton data taken in May 2015 at CDH. The reconstruction employed a filtered back-projection (FBP) followed by an iterated reconstruction (TVS with DROP) that makes use of the tracking information of individual protons to define a most-likely-path (MLP) through the phantom for each.

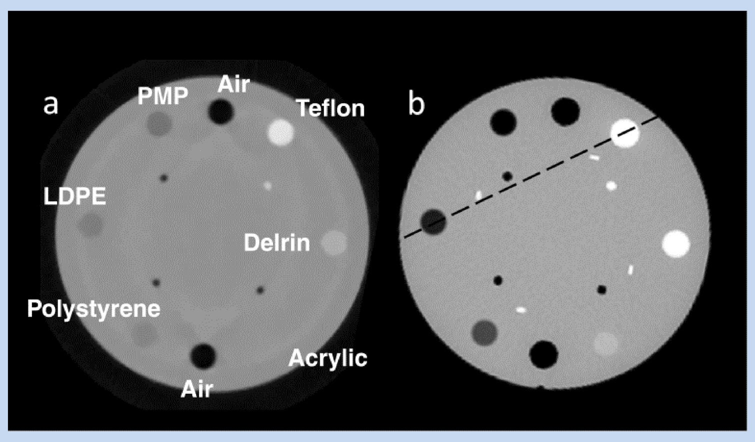

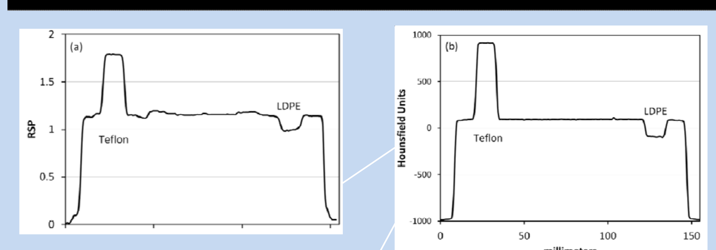

Left (a): A slice of an example CT image reconstructed with data from the completed Phase-II scanner: the CATPHAN 404 module, a cylinder of plastic with several cylindrical inserts of differing materials. The data were collected for 90 stage orientations in 4 degree intervals, with about 3.2 million proton events collected at each angle. Only 51% passed through the reconstruction volume, and 32% of those were rejected by analysis cuts in the data processing. The 3-D image was reconstructed from 99.5 million proton histories, with a voxel size of 0.7 mm x 0.7 mm x 1 mm.)

Right (b): An X-ray CT slice from the same phantom. The dashed line corresponds to the profiles shown below the CT images.

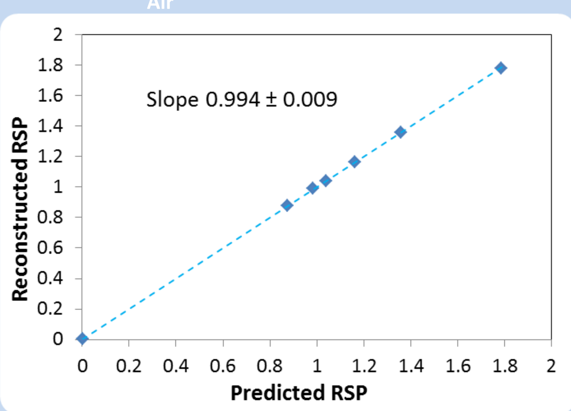

The relative stopping power (RSP) of the variety of materials in the CATPHAN 404 phantom is accurately measured,.

D. C. Williams, "The most likely path of an energetic charged particle through a uniform medium". Phys. Med. Biol. 49 (2004) 2899–2911.

S. Penfold, "Image Reconstruction and Monte Carlo Simulations in the Development of Proton Computed Tomography for applications in Proton Radiation Therapy" PhD thesis Univ. of Wollongong, 2010.

Work is in progress to employ space-carving algorithms to define the reconstruction volume and eliminate the FBP. Progress has also been made on parallelized reconstruction algorithms that run on an array of GPUs. Full reconstructions have been completed in under 8 minutes, similar to the beam time required to acquire the data.

3-D Reconstruction for in-room Position Verification and image-guided Proton Therapy in Progress

3D rendering of the pCT-reconstructed RSP map of a pediatric anthropomorphic head phantom

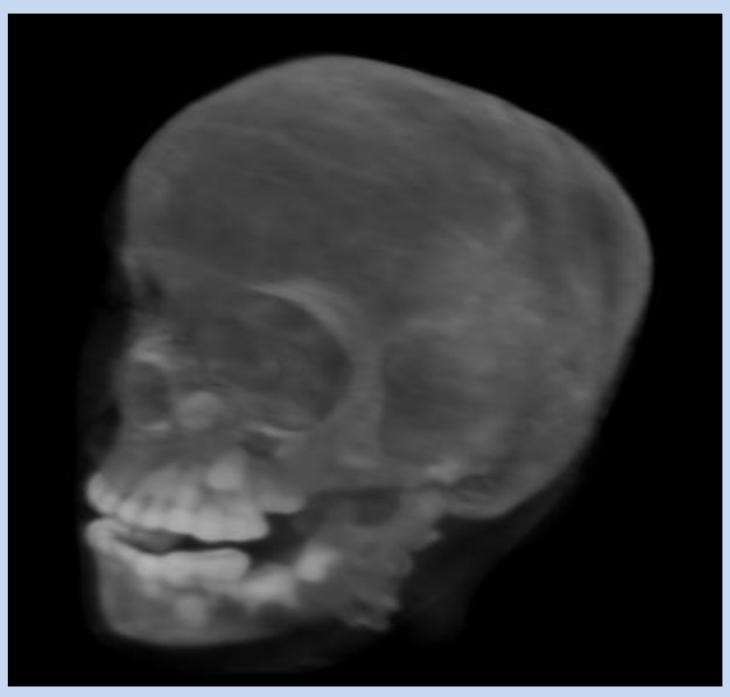

The pCT image of the CIRS head phantom obtained with the Phase II pCT scanner has been tested as input for a 3D-to-3D alignment procedure for treatment-room positioning.

Three cardinal planes of 3D RSP images obtained with Phase II scans of the anthropomorphic head phantom.

Note that these images were taken in two separate scans displaced in the vertical direction.
There are some artifacts in these images, which are currently being addressed in the reconstruction algorithm and in the WEPL calibration, usually the root-cause of artifacts in CT.

V. Bashkirov et al., *Development of proton computed tomography detectors for applications in hadron therapy*, Nucl. Instr. Meth. A (in print)

The authors acknowledge the support of Dr. Mark Pankuch during data taking at CDH.

This work is supported by the National Institute of Biomedical Imaging and Bioengineering (NIBIB) and the NSF, award Number R01EB013118.
The content of this contribution is solely the responsibility of the authors and does not necessarily represent the official views of NIBIB and NIH.